Synthesis and organic solar cell performance of BODIPY and coumarin functionalized SWCNT or graphene oxide nanomaterials

ŞENOCAK, Ahmet, KAYA, Esra Nur, KADEM, Burak, BASOVA, Tamara, DEMIRBAŞ, Erhan, HASSAN, Aseel <http://orcid.org/0000-0002-7891-8087> and DURMUŞ, Mahmut

Published version

ŞENOCAK, Ahmet, KAYA, Esra Nur, KADEM, Burak, BASOVA, Tamara, DEMIRBAŞ, Erhan, HASSAN, Aseel and DURMUŞ, Mahmut (2018). Synthesis and organic solar cell performance of BODIPY and coumarin functionalized SWCNT or graphene oxide nanomaterials. Dalton Transactions, 47 (29), 9617-9626.

Journal Name

ARTICLE

Synthesis and organic solar cell performance of BODIPY and coumarin functionalized SWCNT or graphene oxide nanomaterials

Received 00th January 20xx,
Accepted 00th January 20xx

DOI: 10.1039/x0xx00000x

www.rsc.org/

Ahmet Şenocak[a], Esra Nur Kaya[a], Burak Kadem[b], Tamara Basova[c,d], Erhan Demirbaş[a], Aseel Hassan[e] and Mahmut Durmuş[a]*

The synthesis and characterization of new hybrid materials based on reduced graphene oxide (rGO) or single walled carbon nanotubes (SWCNTs) covalently functionalized by 4,4-difluoro-8-(4-propynyloxy)-phenyl-1,3,5,7-tetramethyl-4-bora-3a,4a-diaza-s-indacene (BODIPY) (**2**) or 7-(prop-2-yn-1-yloxy)-3-(3,4,5-trimethoxyphenyl)-coumarin (**4**) as light harvesting groups were described. The organic solar cell performances of these novel nanomaterials in P3HT:PCBM blend were investigated. These covalently bonded hybrid materials (Reduced graphene oxide:BODIPY (GB), reduced graphene oxide:Coumarin (GC), SWCNTs:BODIPY (CB) and SWCNTs:Coumarin (CC)) were prepared by azide-alkyne Huisgen cycloaddition (Click) reaction between azide bearing SWCNTs or rGO and terminal ethynyl functionalized BODIPY (**2**) or coumarin (**4**) derivatives. The formation of novel nanomaterials was confirmed by the FT-IR, UV-Vis and Raman spectroscopies and thermogravimetric analysis. The best performance on P3HT:PCBM organic solar cell was produced by SWCNTs:Coumarin (CC) hybrids which was coated on a indium tin oxide coated polyethylene terephthalate film (ITO-PET)). The reference device based on P3HT:PCBM blend without CC showed power conversion efficiency (PCE) of 1.16%, FF of 35% and short-circuit current density (Jsc) of 5.51 mA.cm^{-2}. The reference device with CC hybrids within P3HT:PCBM blend increased the values significantly to 1.62% for PCE, 40% for FF and 6.8 mA.cm^{-2} for J_{sc}.

1. Introduction

Due to the rapid developments in societies and increase in energy consumption in line with industrial development and climate change, energy demand is considered as one of the major problems that the world community will face sooner or later [1]. Nowadays, the energy consumption is extremely dependent on fossil fuel resources such as petrol, natural gas and coal. The greatest challenge for the world community is to reduce consumption of fossil fuel specifically by switching it partly and gradually to renewable energies, which therefore requires major developments in the energy infrastructures. Several projects have been carried out by scientists who have particularly identified renewable energy with different resources such as water, wind, bio-materials and solar radiation [2]. Among all these renewable resources, solar energy has drawn an increasing interest of researchers and industry alike [1, 3] due to its viability in applications like powering street lights, distribution around homes, schools, and businesses. The rate of solar radiation intercepted by the earth is about 20,000 times greater than the amount of energy consumed by all human being [4]. Additionally, solar resource exceeds all other renewable alternatives, but breakthrough in the energy generation remains limited because of the high cost and the intermittent nature of solar radiation especially in regions with cold climate. Solar energy technologies are experiencing rapid growth and possibly over the next 40 years they will be one of the leading major global energy providers [2]. The solar radiation comes in the form of electromagnetic radiation of a wide spectrum ranging from high-energy (short wavelength) to low-energy (long-wavelength). The solar spectrum covers ultraviolet (UV) radiation ranging from 100-400 nm, visible radiation ranging from 400-700 nm and infrared (IR) radiation (700 nm and above). The UV, visible and infrared radiations are significant parts of the solar spectrum, which play an important role in global solar energy application including solar thermal and photovoltaics (PV). Up to date, different types of solar cells have been demonstrated in classed in three different generations; the distinction between these generations basically lays in the kinds of materials used. The first generation consists of cells prepared by using crystalline silicon (Si) whereas the second generation solar cell is based on semiconductor thin film technology; these include amorphous silicon (a-Si), polycrystalline silicon, copper indium gallium selenide (CIGS) and cadmium telluride (CdTe) based solar cells. The third generation of solar cells is based on a

[a]*Gebze Technical University, Department of Chemistry, Gebze, Kocaeli 41400, Turkey*
[b]*Department of Physics, College of Science, University of Babylon, Iraq*
[c]*Nikolaev Institutes of Inorganic Chemistry SB RAS, Lavrentiev Pr. 3, Novosibirsk 630090, Russia*
[d]*Novosibirsk State University, Pirogova Str. 2, Russia*
[e]*Material and Engineering Research Institute, Sheffield Hallam University, UK*
† *Footnotes relating to the title and/or authors should appear here.*
Electronic Supplementary Information (ESI) available: [details of any supplementary information available should be included here]. See DOI: 10.1039/x0xx00000x

range of new materials, such as organic polymers, small molecules, nanotubes, quantum dots, silicon nanowires, and organic dyes [5]. Organic solar cells (OSCs) are considered as promising cost-effective, lightweight and suitable for role-to-role technology which can be prepared via simple solution processing methods on flexible substrates [6]. Among several organic materials, the poly(3-hexylthiophene) (P3HT) and [6,6]-phenyl C61-butyric acid methyl ester (PCBM) bulk heterojunction (BHJ) blends are the most investigated donor/acceptor materials in OSCs [7, 8]. The nanoscale interpenetrated network morphology of the P3HT:PCBM blend is a crucial factor in order to achieve higher solar cell performance, through facilitating charge carriers separation and transfer, where the exciton diffusion length is in the range between 10-20 nm [9]. Furthermore, ternary blends are considered as an encouraging model to increase OSCs performance by either increasing charge carriers' mobility or incorporation of complementary optical materials or both. The incorporation of functional materials such as single-walled carbon nanotubes (SWCNTs) and reduced graphene oxide (rGO) or graphene with unique properties are promising materials for ternary blend composites [10]. In a recent research, it has been shown that the use of carbon based hybrids has resulted in enhancing the performance of P3HT:PCBM based OSCs to achieve 5.3% compared to 3.5% for a reference P3HT:PCBM based device [11]. Generally, SWCNTs and rGO might have some drawbacks when they are added to the active layer due to the possible contribution in compromising the device shunt resistance, as well as acting as charge recombination centers [11]. Therefore, small proportions of carbon-based functional materials are used in ternary blends-based OSCs.

In the current study, new hybrids based on single walled carbon nanotubes (SWCNTs) or reduced graphene oxide (rGO) functionalized with BODIPY and coumarin derivatives (Scheme 1) have been synthesized and investigated to enhance the performance of P3HT:PCBM based OSCs. With keep this in mind, we have focused on BODIPY and coumarin functionalized nanocarbon hybrids based OSCs. These molecules show outstanding photophysical properties such as a high molar extinction coefficient of absorbance, high fluorescence quantum yield, and excellent photostability. BODIPY has excellent performance as a functional dyes applied in chemosensors, [12] bioprobes, [13] photodynamic therapy, [14] organic light-emitting diodes, [15] and solar cell devices [16]. Coumarin derivatives are also widely used as commercially significant organic fluorescent materials having, due to their large stokes shift, sufficient fluorescence in the visible light range, good solubility and high fluorescence quantum yield. Moreover, coumarin based dyes with their good photo-response in the presence of visible region, long term stability under 1 sun illumination, appropriate located LUMO level have given better performance in photovoltaic devices [17].

2. Experimental

2.1. Materials and methods

All reagents and solvents are of reagent grade quality and are obtained from commercial suppliers; 3,4,5-Trimethoxyphenylacetic acid and 2,4-dihydroxybenzaldehyde were purchased from Sigma-Aldrich and sodium L-ascorbate were purchased from Alfa Aeser. SWCNTs were purchased from Sigma-Aldrich. Sodium azide and copper(II) sulfate pentahydrate were supplied from Merck. Reduced graphene oxide used as a graphene nanomaterial was obtained from Zerre the brand of Hazerfen KMETSTAŞ (Hazarfen Chemicals Materials and Energy Technologies and Trade Inc.) Company, Turkey. The surface area of this rGO as deduced from BET measurements (Quantachrome Instruments) and the ratio of C:O from Scanning electron microscopy with energy dispersive X-ray spectroscopy (SEM-EDX, Philips XL 30 SFEG) were measured as 565 m^2/g and 4.77, respectively. The number of layers determined from Atomic Force Microscopy (AFM, Digital Instruments) and Transmission Electron Microscopy (TEM, Tecnai G2 F20 S-TWIN) was in the range of 4–7 sheets and the lateral size of rGO flake was approximately 5 µm. Moreover, for solar cell application, the following materials have been used to prepare the solar cell devices: poly (3-hexathiophine-2,5-diyl) (P3HT), [6,6]-phenyl C61 butyric acid methyl ester (PCBM), poly (3,4-ethylenedioxythiophene) polystyrene sulfonate (PEDOT:PSS) 1.3 wt% dispersion in H_2O (conductive grade), chlorobenzene (CB) and chloroform (CF) were purchased from Sigma-Aldrich and used without any further purification. ITO-coated glass slides (sheet resistant of 8-12 Ω/sq) were also purchased from Sigma-Aldrich.

2.2. Synthesis

(4,4'-Difluoro-8-(4-hydroxy)-phenyl-1,3,5,7-tetramethyl-4-bora-3a, 4a-diaza-s-indacene (**1**)) [18] was synthesized and purified according to literature procedure. 4,4'-Difluoro-8-(4-propynyloxy)-phenyl-1,3,5,7-tetramethyl-4-bora-3a,4a-diaza-s-indacene (**2**) (BODIPY) was synthesized and purified according to literature procedures [19, 20]. 7-Hydroxy-3-(3,4,5-trimethoxyphenyl) coumarin (**3**) was synthesized and purified according to literature procedure [21].

2.2.1. 7-(Prop-2-yn-1-yloxy)-3-(3,4,5-trimethoxyphenyl)-coumarin (**4**)

Compound **3** (400 mg, 1.218 mmol) dissolved in 20 mL DMF and propargyl bromide (0.02 mL, 1.827 mmol) was added to this solution. After stirring 10 min, K_2CO_3 (252 mg, 1.827 mmol) was added to this solution. The reaction mixture was heated at 60 ^{o}C for 24 h under argon atmosphere. Then the resulting mixture was poured into ice water. The precipitate was filtered, washed with water and dried. The crude product was purified by column chromatography using dichloromethane as an eluent. Yield: 57%; UV-Vis: (THF, $1x10^{-5}$M) λ_{max}: 350 nm; FTIR: (ν_{max}/cm^{-1}) 3260 (≡CH), 3035-3007 (Ar–CH), 2943–2829 (aliphatic –CH), 1719 (C=O lactone), 1607–1461 (C=C), 1218–1121 (Ar–O–C); ^{1}H NMR (500 MHz; chloroform-d_1): δH, ppm: 7.76 (s, 1H, lactone H), 7.49 (d, 1H, J=8.5 Hz, Ar-H), 7.00 (s, 1H, Ar-H), 6.96 (dd, 1H, J=8.7 and 2.0 Hz, Ar-H), 6.94 (s, 2H, Ar-H), 4.80 (d, 2H, J=1.88Hz, Al-CH_2),

3.93 (s, 6H, -OCH_3), 3.90 (s, 3H, -OCH_3), 2.60 (s, 1H, ≡CH); MALDI-TOF (m/z) calc. 366.37, found: $[M+H]^+$ 366.104, $[M+Na]^+$ 389.38 (Fig. S1).

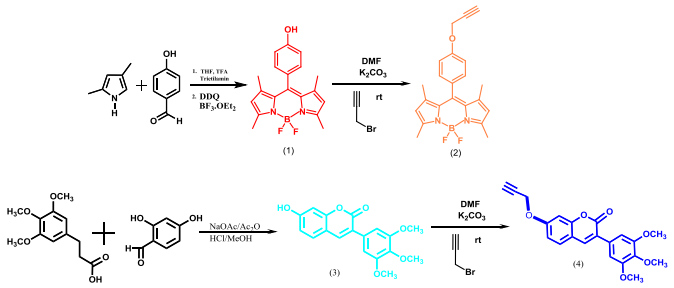

Scheme 1. Synthetic pathway of ethynyl BODIPY (**2**) and coumarin (**4**).

2.3. Preparations of SWCNT-N_3 and rGO-N_3

SWCNT-N_3 and rGO-N_3 were synthesized according to the method given in the literature [22]. 250 mg (3.84 mmol) NaN_3 and 165 mg (1.01 mmol) iodine monochloride were dissolved in 25 mL of acetonitrile (ACN) under nitrogen atmosphere. This mixture was magnetically stirred for 15 min at 0°C followed by adding 20 mg SWCNTs or graphene to the solution; the reaction was stirred at room temperature for 24 hours and filtered off. The solid products were washed with DMF and ethanol to remove excess unreacted compounds and dried under vacuum.

2.4. Preparation of hybrids (CB, CC, GB and GC)

Hybrid materials were synthesized according to the modified method described in our earlier publication [22]. 20 mg (0.012 mmol) of BODIPY 2 or coumarin 4, was dissolved in 2 mL DMF separately and then sonicated for 15 min at room temperature. On the other hand, 5 mg SWCNT-N_3 (or rGO-N_3) was suspended separately in 2 mL DMF and sonicated for 30 min at room temperature; BODIPY (2) or coumarin (4), solutions were then added drop wise to SWCNT-N_3 (or rGO-N_3) suspension. To this suspension, 1.0 mol% copper(II) sulfate pentahydrate and 5.0 mol% sodium L-ascorbate in 1 mL water were added at room temperature as catalysts and the resulting mixture was kept overnight at 90 °C. Finally, the reaction mixture was centrifuged twice with water, ethanol and dichloromethane in sequence and dried in vacuum. Synthetic pathway of graphene or SWCNT hybrids is shown in Scheme 2.

FTIR spectrum:

SWCNTs:BODIPY (CB) hybrid (ν_{max}/cm^{-1}), 3180 (Triazole ring CH), 3040 (Aromatic CH), 2984–2843 (Aliphatic CH), 1620 (C=C), 1494 (B-N), 1336 (Aliphatic CH), 1240 (Aromatic CH), 1089 (C–O–C).

SWCNTs:Coumarin (CC) hybrid (ν_{max}/cm^{-1}), 3240 (Triazole ring C=H), 3070 (Aromatic CH), 2980–2903 (Aliphatic CH), 1665 (C=O), 1617 (C=C), 1360 (Aliphatic CH), 1235 (Aromatic CH), 1046 (C–O–C)

Reduced Graphene Oxide:BODIPY (GB) hybrid (ν_{max}/cm^{-1}), 3197 (Triazole ring CH), 3058 (Aromatic CH), 2922–2853 (Aliphatic CH), 1596 (C=C), 1503 (B-N), 1355 (Aliphatic CH), 1223 (Aromatic CH), 1102 (C–O–C).

Reduced Graphene Oxide:Coumarin (GC) hybrid (ν_{max}/cm^{-1}), 3195 (Triazole ring C=H), 3077 (Aromatic CH), 2966–2820 (Aliphatic CH), 1720 (C=O), 1621 (C=C), 1355 (Aliphatic CH), 1226 (Aromatic CH), 1120 (C–O–C).

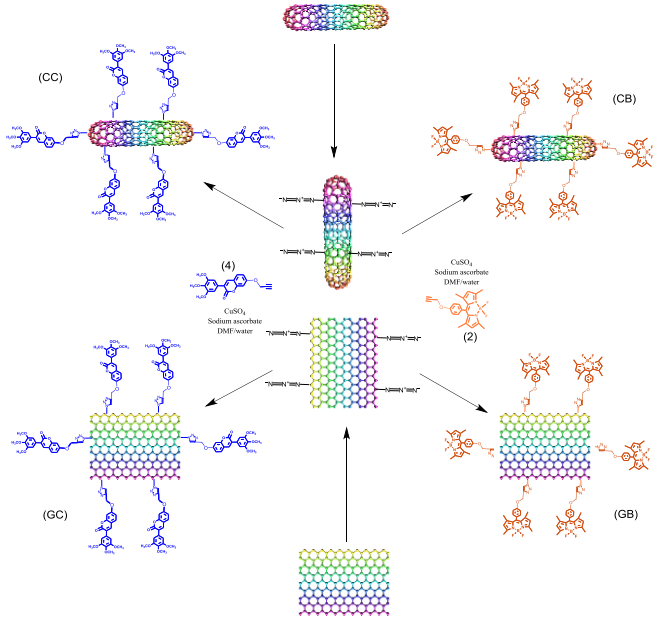

Scheme 2. Synthetic pathway of graphene and SWCNT hybrid materials.

2.5. Characterization techniques

BODIPY, coumarin, SWCNTs and rGO as hybrids were examined using different techniques such as FT-IR, Raman spectroscopy, UV-Vis absorption spectroscopy, ^{1}H-NMR, MALDI mass spectra, SEM, cyclic voltammetry and electrical conductivity measurements. FT-IR spectra were recorded on a Perkin Elmer Spectrum 100 spectrophotometer. Raman spectra were recorded with a Triplemate, SPEX spectrometer equipped with CCD detector in back-scattering geometry. The 488 nm, 40 mW line of Ar-laser was used for the spectral excitation. ^{1}H-NMR spectra with tetramethylsilane (TMS) as an internal standard were recorded on a Varian 500 MHz spectrometer. The mass spectra were recorded on a Matrix Assisted Laser Desorption Ionization (MALDI) BRUKER Microflex LT using 2,5-dihydroxybenzoic acid (DHB) as matrix. UV-visible spectrophotometer (Varian 50-scan UV–visible) in the range of 190-1100 nm was used to measure the absorption spectra. The morphologies of synthesized hybrids were determined by FEI-Nova scanning electron microscopy (SEM). The cyclic voltammetry and square wave voltammetry measurements were carried out with CH Instruments 440B Electrochemical analyzer utilizing a three-electrode configuration at 25 °C [23]. The working electrode was glassy carbon electrode. A Pt wire served as the counter electrode. Saturated calomel electrode (SCE) employed as the reference electrode was separated from the bulk of the solution by a double bridge. Electrochemical grade tetrabutylammonium perchlorate (TBAP) was employed as the supporting

electrolyte in voltammetric measurements in extra pure dichloromethane (DCM) at a concentration of 0.10 mol dm^{-3}. High purity N_2 was used to deoxygenate the solution at least 10 minutes prior to each run and maintains a nitrogen blanket. All theoretical calculations were performed by using Gaussian 09 suite program [24]. The molecular geometries of the BODIPY and coumarin compounds were optimized by the density functional theory (DFT) - B3LYP/6-311G(d,p) basis set. The excited states were calculated by using time-dependent density functional theory (TD-DFT calculations) B3LYP/6-311G(d,p) and B3PW91/6-311G (d,p) in DCM [25]. The molecular orbital contours were visualized using Gauss view 5.0.9. The thickness of the deposited layers was determined using M2000 (J.A. Woollam Co., Inc.) spectroscopic ellipsometer operating in the wavelength range 370-1000 nm. The photovoltaic properties in the form of current density-voltage (J-V) dependence were measured using 4200 Keithley semiconductor characterization system and the photo current was generated under AM 1.5 solar simulator source of 100 $mW.cm^{-2}$. The fill factor (FF) and the overall light to-electrical power conversion efficiency (PCE) of the solar cells were determined according to the following equations [26]:

$$PCE(\%) = \frac{J_{max} \times V_{max}}{P_{in}} \quad (1)$$

$$FF = \frac{J_{max} \times V_{max}}{J_{sc} \times V_{oc}} \quad (2)$$

where J_{sc} is the short-circuit current density ($mA.cm^{-2}$), V_{oc} is the open-circuit voltage which is generally defined as the difference between the HOMO donor and LUMO acceptor [27], P_{in} is the incident light power and J_{max} ($mA.cm^{-2}$) and V_{max} (V) are the current density and voltage at the point of maximum power output in the J-V curves, respectively.

2.6. Organic solar cells fabrication

P3HT:PCBM blends were mixed with functionalised carbon nanomaterials to produce a ternary active layer blends in the concentration ratio of 0.01mg:14mg of functionalised carbon nanomaterials to the P3HT:PCBM blend as higher concentrations may result in device failure through short circuit; these hybrids were dissolved in a co-solvent comprising CB and CF in the ratio 1:1 [28]. The solutions were stirred overnight at 45°C prior to film deposition. ITO coated glass slides were cleaned using deionised water, acetone and 2-propanol for 10 min each in ultrasonic bath, respectively, and then blown dry in N_2 gas. PEDOT:PSS layers were spin coated on the clean ITO substrates at 2000 rpm for 30 sec, followed by heat-treatment at 150°C for 10 min in ambient air. Subsequently, PEDOT:PSS layers coated ITO substrates were transferred to a nitrogen-filled glove box where the active layers were spin coated at 1500 rpm for 30 sec to obtain a thickness of ~150 nm and then heat-treated inside the glove box at 120 °C for 10 min. Aluminium (Al) was thermally evaporated as a back electrode using Edward thermal deposition system with a thickness of ~100 nm under vacuum of ~$2x10^{-6}$ mbar, at the deposition rate of 0.1-0.2 $nm.sec^{-1}$ as was detected by a quartz crystal thickness monitor. All final devices were subjected to further heat-treatment inside the nitrogen-filled glove box at 120°C for 10 min.

3. Results and discussion

3.1. Synthesis and characterization of BODIPY and coumarin derivatives

Compound 2 (Scheme 1) was synthesized and purified according to literature procedure [20]. Compound 3 was also synthesized and purified according to literature procedure [21]. The novel 7-(prop-2-yn-1-yloxy)-3-(3,4,5-trimethoxyphenyl)-coumarin was prepared by the reaction of 7-hydroxy-3-(3,4,5-trimethoxyphenyl)coumarin with propargyl bromide in DMF. SWCNTs and rGO bearing azido groups were synthesized by the reaction of SWCNTs or rGO with sodium azide in the presence of iodine monochloride in acetonitrile (Scheme 2). The target SWCNTs and rGO hybrid materials CB, CC, GB and GC were prepared through the reaction of azido substituted SWCNTs or rGO with the newly synthesized terminal ethynyl bearing coumarin or BODIPY derivatives by azide-alkyne Huisgen cycloaddition (Click) reaction in DMF using copper(II) sulfate pentahydrate and sodium L-ascorbate as catalysts (Scheme 2).

The ^{1}H-NMR spectrum of the compound 4 was recorded in $CDCl_3$ solution (Fig. S2, Supporting Information). The ethynyl proton was observed at 2.60 ppm as a singlet. The methoxy protons were observed at 3.90 and 3.93 ppm as singlet peaks. The aliphatic protons of CH_2 group were observed at 4.80 ppm as a doublet. The proton in the fourth position of coumarin lactone ring was observed at 7.76 ppm as a singlet. The aromatic protons were observed at 7.49, 7.00, 6.96 and 6.94 ppm as doublet, singlet, double doublet and singlet, respectively.

3.2. Characterization of BODIPY and coumarin functionalized SWCNT and rGO hybrid nanomaterials

3.2.1. Vibrational spectra study

Hybrid nanomaterials of BODIPY and coumarin functionalized SWCNT and rGO were obtained as powders. SEM images of the films of the novel hybrids are shown in Fig. S3. GC and GB films have demonstrated flakes like features, while tube like features have been observed in the case of CC and CB hybrids. Formation of CB, CC, GB and GC hybrid nanomaterials was confirmed by the methods of IR and Raman spectroscopy. Fig. 1 shows the FT-IR spectra of free BODIPY, free coumarin, rGO-N3, SWCNT–N_3, CB, CC, GB and GC hybrids. BODIPY compound exhibited vibration peaks at 3261 and 1491 cm^{-1} assigned to C≡CH and B-N stretching vibrations, respectively. Additionally, coumarin compounds exhibited vibration peaks at 3260, 1719 and 1218 cm^{-1} assigned to C≡CH, C=O lactone and Ar–O–C stretching, respectively. On the other hand, the addition of N_3 groups to SWCNTs or rGO was identified with the observation of a peak at 2100 cm^{-1} for the –N=N=N (azide) vibration in the FT-IR spectra of SWCNTs–N_3 or rGO–N_3. The ≡CH peaks in the

FT-IR spectra of BODIPY and coumarin compounds and N_3 peaks for SWCNT–N_3 or rGO–N_3 compounds disappeared after formation of hybrid nanomaterials (Fig. 1). Additionally, the vibration peak for the CH stretching of the triazole ring, observed at about 3200 cm^{-1} for all hybrids (Fig. S4), was another proof for the functionalization of SWCNTs or rGO with BODIPY or coumarin moieties.

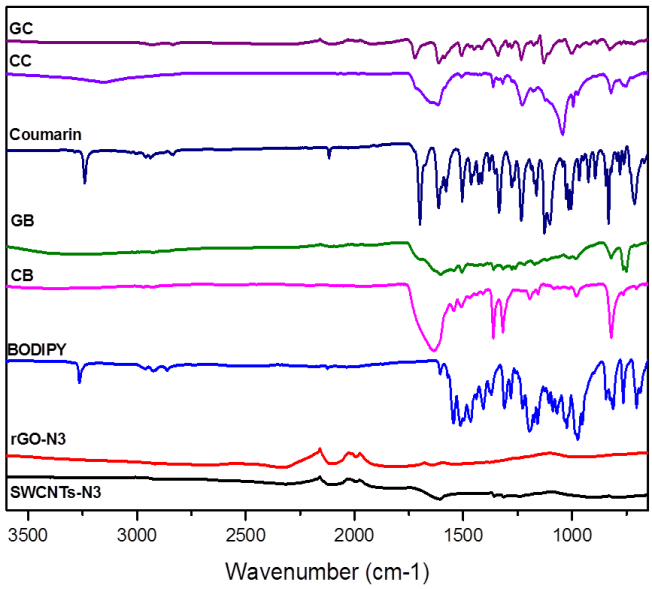

Figure 1. FTIR spectra of SWCNTs-N3, rGO-N3, pristine BODIPY, pristine coumarin and their CB, GB, CC and GC hybrids.

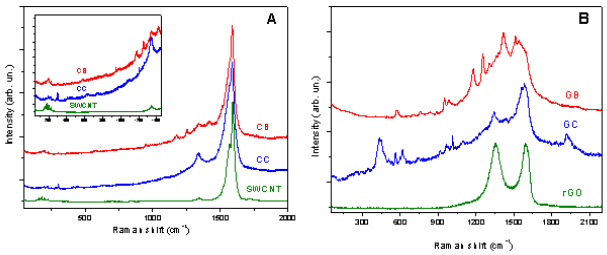

Figure 2. (A) Raman spectra of pristine SWCNT and its CC and CB hybrids in the range 50-2000 cm-1 and (B) Raman spectra of pristine rGO and its GC and GB hybrids.

Raman spectra of SWCNT, CC and CB hybrids are shown in Fig. 2 (A), while Raman spectra of rGO and its GC and GB hybrids are presented in Fig. 2(B). The spectra of both SWCNT and the hybrids (Fig. 2(A)) contain the characteristic peaks typical for carbon nanomaterials, namely the D band at around 1340 cm^{-1} (disorder mode) and the G band (tangential mode) at 1592 cm^{-1} [29]. The I_D/I_G ratio has a value of 0.04 in the spectrum of pure SWCNT, while the values of 0.20 and 0.15 were obtained from the spectra of CC and CB, respectively. The inset of Fig. 2(A) shows the enlarged part of the spectrum from 50 to 1470 cm^{-1}. The characteristic bands corresponding to vibrations of coumarin and BODIPY moieties are noticeable in the spectra of CC and CB (Fig. 2(A), inset). Comparison of the hybrid spectra with those of coumarin and BODIPY shows that some characteristic vibrations of coumarin and BODIPY moieties are shifted noticeably due to the covalent bonding with SWCNT. The RBMs of SWCNT in the range 158-304 cm^{-1} (Fig. 2(A)) are ascribed to a distribution of diameters in the SWCNTs [30], which corresponds to nanotube diameters in the range 0.7 to 1.4 nm. Considerable changes are observed in the spectra of CC and CB in the range of RBM modes. The intensities of most of RBMs decreased and only two bands at 199 and 221 cm^{-1} in the spectrum of CC and three bands at 164, 200 and 222 cm^{-1} in the spectrum of CB remain pronounced. rGO sample displays two peaks at 1358 cm^{-1} and 1598 cm^{-1} corresponding to D band and G bands, respectively (Fig. 2 (B)). In contrast to the case of rGO, the G bands in GC and GB spectra shift to 1586 cm^{-1}. The low-frequency peak shift is assigned to the interaction between coumarin and BODIPY moieties with rGO sheets. The noticeable change of I_D/I_G ratio provides further indication of rGO functionalisation. Moreover, there are many bands corresponding to coumarin and BODIPY moieties overlap with D band and G bands of rGO, thus indicating that coumarin and BODIPY molecules are attached to the carbon nanomaterials.

3.2.2. Thermogravimetric analysis

Thermal stability of the hybrids in comparison with pristine BODIPY, coumarin, SWCNTs, and rGO were examined by TGA weight loss near 100 °C, as the samples were completely dried before testing to eliminate the influence of absorbed moisture on the results. Fig. 3 presents TGA thermograms, recorded under N_2 atmosphere. The TGA data show weight loss for pristine SWCNTs, rGO, SWCNT-N_3, rGO-N_3, CB, CC, GB, GC, BODIPY and coumarin at 800 °C; those are 4.70, 11.51, 12.68, 32.18, 28.43, 30.13, 41.46, 50.48, 50.07 and 63.65%, respectively. The thermograms of pristine SWCNTs, SWCNT-N_3, rGO and rGO-N_3 revealed its excellent thermal resistance up to 800 °C. Weight losses due to the functional groups on SWCNTs were estimated to be 8.43, 17.45 and 15.75% for SWCNT-N_3, CC and CB, respectively. The number of the azide groups on the SWCNTs were calculated as described in the literature [31]. The number of azide functional groups in SWCNT-N_3 was estimated as 1 per 38 carbon atoms. The amount of coumarin molecules covalently anchored on the surface of the nanotubes as a real ratio was 27.41% (17.45%/63.65%). It was estimated that CC contains one coumarin molecule per 81 carbon atoms according to the calculation of (72.59%x366.10)/(27.41%x12). Similarly, the amount of BODIPY molecules bonded on the surface of the nanotubes as a real ratio was 31.45% (15.75%/50.07%). It was calculated that CB contains one BODIPY molecule per 69 carbon atoms according to the calculation of ((72.59%x366.10)/(27.41%x12)). In addition, the number of azide functional groups in rGO-N_3 was 1 per 14 carbon atoms and the amounts of coumarin and BODIPY bonded on rGO as a real ratios were 28.75% (18.30%/63.65%) and 18.53% (9.28%/50.07%), respectively. The calculations indicated that GC contained one coumarin per 76 C atoms and GB contained one BODIPY per 138 C atoms. TGA results showed that hybrid materials were more stable than BODIPY and coumarin. This could be explained by the thermal stability of the hybrids after functionalization by

BODIPY or coumarin groups that makes them useful materials for applications in electronic devices [31].

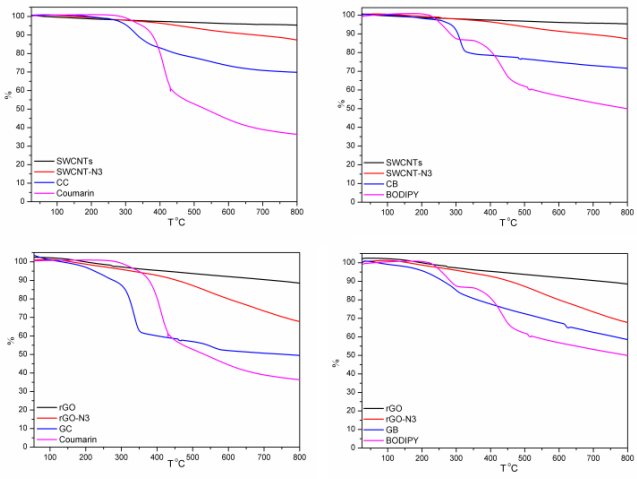

Figure 3. Thermogravimetric analysis of CC, CB, GC and GB in comparison with pristine SWCNTs, SWCNT-N_3, rGO, rGO-N_3 and compounds 2 and 4.

3.2.3. Studies of the HOMO-LUMO transitions

Coumarin and BODIPY functionalized SWCNTs and rGO hybrid nanomaterials (CB, CC, GB and GC) were dispersed in DMF (0.25 mg/mL^{-1}); 20 µL from each solution was added to 3 mL DMF for investigation of optical absorption spectra. While pristine BODIPY and coumarin derivatives (2 and 4) are soluble in DMF, their hybrids (CC, CB, GC and GB) exhibited good dispersion in this solvent (Fig. S5). The UV–Visible absorption spectra of CC, CB, GC and GB hybrids compared to those of pristine BODIPY and coumarin derivatives are shown in Fig. 4.

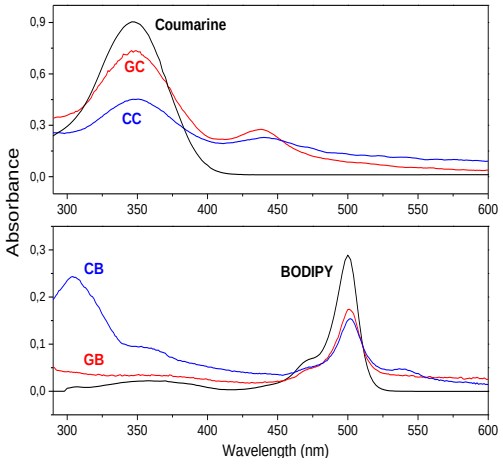

Figure 4. UV-Vis spectra of the compounds 2, 4 and their hybrids CB, CC, GB and GC.

The UV–Visible absorption spectra of CC, CB, GC and GB hybrids compared to those of pristine BODIPY and coumarin derivatives are shown in Fig. 4. The spectra of BODIPY and coumarin compounds showed characteristic absorptions at 500 and 347 nm, respectively. Small bathochromic shift (2-3 nm) of the absorption bands in the spectra of the hybrids compared to pristine BODIPY and coumarin was observed, while the absorption intensities decreased with the absorption bands appeared broadened. Presumably the shift of the bands is not significant because the interaction of carbon nanomaterials with BODIPY or coumarin *via* formation of triazole ring does not affect the aromatic systems of the molecules and consequently does not much alter their electronic properties. It was revealed that such spectra give an obvious indication of the ground-state electronic interactions between BODIPY or coumarin and graphene or SWCNTs within the hybrid materials. The broad coverage of the absorption spectra over the UV–Vis-NIR regions could result in improved light-harvesting properties [32]. The energy band gaps (E_g) of BODIPY, coumarin and their hybrids with rGO or SWCNTs were estimated using intersection points of absorption and emission spectra of thin films of the investigated compounds (Table S1). BODIPY and coumarin exhibited band gaps E_g = 2.44 and 2.85 eV, respectively. The band gaps for CB, CC, GB and GC hybrids were 2.39, 2.77, 2.37 and 2.80 eV, respectively. These optical band gap values indicated that these hybrid materials are potentially applicable as solar cell materials.

For a better understanding of the structural and electronic features of these molecules, the DFT theoretical calculations were further performed, and the optimized structures and the electronic distribution in the HOMO and LUMO levels are presented in Fig. S6. All calculations were carried out with the Gaussian 09 program suite by using the B3LYP and B3PW91 methods and 6-311 G (d,p) and basis set. The optimized ground-state geometries of these molecules are shown in Fig. S6. The electron distributions of BODIPY and coumarin were 2.89 and 3.39 for B3LYP/6-311G (d,p) indicating that the π-electrons in the HOMO are delocalized over the entire molecule backbone offering effective orbital interactions among the stacked π–systems. Computational band gaps have close values to the optical and electrical band gaps. These results indicate that hybrid materials prepared from these molecules are also potentially applicable in PV applications.

The cyclic voltammograms of BODIPY and coumarin are illustrated in Fig. S7. As shown in this figure, BODIPY presents reversible onset oxidation potential at around 1.22 V, and a reversible reduction at around -1.17 V. The coumarin compound presents a reversible oxidation and a reversible reduction potential at 1.22 and -1.71 V, respectively. The cyclic voltammograms of CC, CB, GC and GB hybrids are illustrated in Fig. S8 and the values are presented in Table S1. As shown in this figure, CB and GB exhibit irreversible onset oxidation potentials at around 0.81 and 0.83 V, and irreversible reductions at around -1.04 and -0.77 V. The coumarin based hybrids (CC and GC) revealed irreversible oxidation and irreversible reduction potentials at 1.31, 1.17 V and -1.35, -1.26 V, respectively.

The HOMO and low LUMO energy levels of the materials were calculated and the results are presented in Table S1. The corresponding HOMO energy level of BODIPY, coumarin, CC, CB, GC and GB hybrids were calculated as -5.88, -5.95, -6.04, -5.54, -5.90, and -5.56 eV from the equation E_{HOMO} (eV) = -(E_{ox}^{onset} - $E_{Fc/Fc+}^{onset}$)-5.13 eV [33]. The LUMO energy levels of these compounds were determined as -3.56, -3.02, -3.38, -

3.69, -3.47 and -3.96 eV, respectively from the following equation: E_{LUMO} (eV) = - (E_{red}^{onset} - $E_{Fc/Fc+}^{onset}$) -5.13 eV (Table S1). These hybrids are actually located at very low energy level, which is an attractive property in bulk-heterojunction (BHJ) solar cell device. Different oxidation and reduction peaks were exhibited by the different hybrids in the scanned electrochemical window. Coumarin and BODIPY bonded with SWCNTs or rGO exhibited broadened redox peaks which were attributed to low solubility and strong aggregation in solution. Fig. 5 shows energy level alignments of BODIPY, coumarin and their hybrids. The energy levels alignment was assumed to be occurring between P3HT/CC, P3HT/CB, P3HT/GC and P3HT/GB. It was known that the main mechanisms in the OSCs operation are based on exciton generation, separation and dissociation with charge separation mainly taking place at the interface between the two materials (donor/acceptor) within the blends. Carbon-based hybrids are also likely to act as p-type materials, and it was demonstrated that P3HT/SWCNTs and P3HT/rGO hybrids may act as hole transport layers.

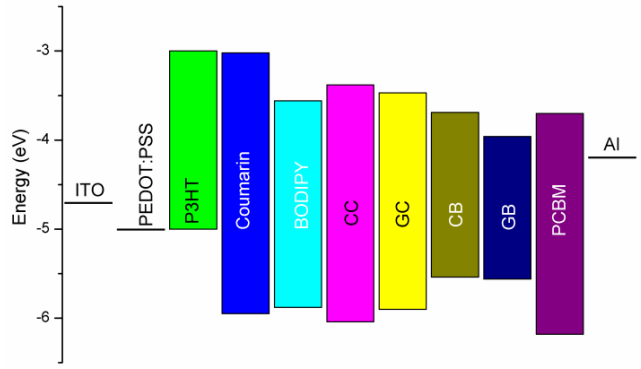

Figure 5. Determined energy diagram with HOMO/LUMO levels of coumarin, BODIPY, CC, GC, CB and GB in a BHJ OSC device

3.3. Study of solar cell properties

To investigate the solar cell performances, thin films of P3HT:PCBM blended with the novel hybrids (Reduced graphene oxide:BODIPY (GB), reduced graphene oxide:Coumarin (GC), SWCNTs:BODIPY (CB) and SWCNTs:Coumarin (CC)) were prepared. The absorption spectra of the P3HT:PCBM films with and without the addition of the hybrids is shown in Fig 6. Typical absorption spectra have been observed for the P3HT:PCBM blends with four different bands [34]. Bands a, b and c were attributed to the absorption spectra of the P3HT whereas band d is ascribed to the absorption spectrum of the PCBM [11]. The ternary blend is well-known as a promising concept to improve the OSCs performance, which could be achieved by either incorporation of complementary optical material or a material with higher charge carrier mobility or both [11]. The effect on of the absorption properties of P3HT:PCBM blends as a result of adding a small portion of the studied hybrids has been analyzed. All the studied hybrids have shown no clear change or shift in the absorption peaks of the P3HT:PCBM due to the small addition of the hybrids within the P3HT:PCBM blend. It is worth noting that the band gap and the energy levels alignment of the P3HT:PCBM blends might result in enhancing the light absorption properties [35]. The optimization of carbon-based blends used in OSCs could be attained when small proportions of these materials are used. However, the use of SWCNTs or rGO has some drawbacks in solar cell applications such as their possible contribution in compromising the device shunt resistance, as well as acting as charge recombination centres [36].

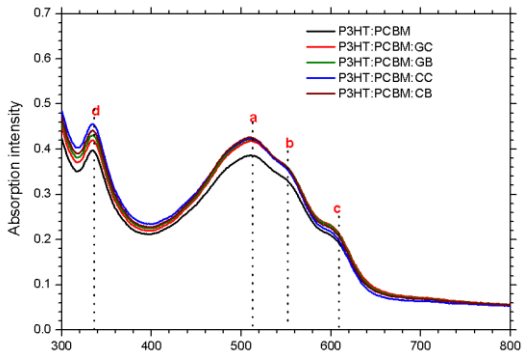

Figure 6. Absorption spectra of the P3HT:PCBM pure and blended with Reduced Graphene Oxide:BODIPY (GB), Reduced Graphene Oxide:Cumarine (GC), SWCNTs, BODIPY (CB) and SWCNTs:Cumarine (CC) hybrids.

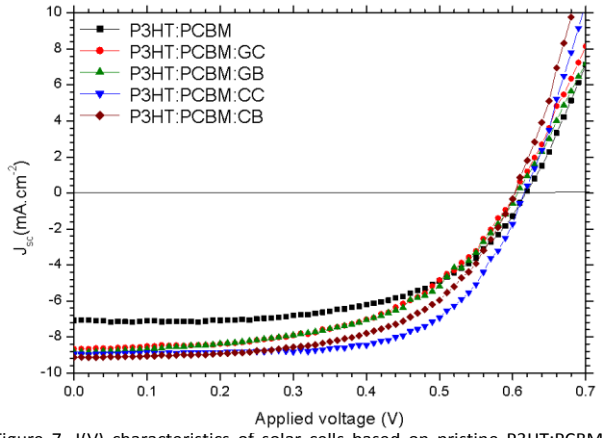

Figure 7. J(V) characteristics of solar cells based on pristine P3HT:PCBM blend and P3HT:PCBM-hybrids ternary blends.

The photovoltaic properties of the novel GB, GC, CB and CC hybrids have been investigated as ternary blends with P3HT:PCBM, separately, as shown in Fig.7; results of the PV characteristics are summarized in Table 1. The new hybrids (GB, GC, CB and CC) were added to the main (P3HT:PCBM) blends in a small portions in order to avoid any possible short-circuit as the hybrids are based on carbon based materials [37]. The reference device based on pure P3HT:PCBM blend has displayed a PCE of 2.62% with FF of 60% and J_{sc} of 7.1 mA.cm^{-2}. P3HT:PCBM:GB based device has shown a PCE of 2.9% with J_{sc} of 8.8 mA.cm^{-2} V_{oc} of 0.6 and FF of 55%. On the other hand P3HT:PCBM:CB based device has exhibited an increase in the J_{sc} to 9.1 mA.cm^{-2} and no change in the device V_{oc}, whereas FF has increased to 59% and the PCE increased to 3.22. The increase in the PCE is mainly attributed to the increase in the current density which is in turn might be ascribed to the addition of the BODIPY group within the P3HT:PCBM blend. Recently, BODIPY dyes are used in dye sensitized solar cell (DSCs) applications due to their strong

absorption and fluorescence in the visible and the near-infrared regions [38, 39]. A solar cell device may be affected by many factors, including aggregation, light absorption coverage, loading density, frontier molecular orbital energy levels as well as redox couple potential. Moreover, the PCE is the result of a global optimization of various processes. For example, a dye with a broader light absorption can harvest more photons for electron generation, which was achieved by lowering LUMO or increasing HOMO levels [40]. CB and GB have a broad absorption and narrow band gaps with lower LUMO and higher HOMO than pristine BODIPY dye, thus PCE of hybrid materials increased considerably.

Also, the functional carbon based groups have clear influence on the device performance due to their unique properties, especially, the nanoscale interpenetrated network and the electrical conductivity which might result in efficient charge transfer within the blend and thus improving the PCE [41, 42]. The latter improvements could also contribute to enhance the shunt resistance by creating percolation pathways which facilitate charge carriers' transport and increase the short circuit current density [42]. Furthermore, P3HT:PCBM:GC based device has demonstrated a PCE of 2.85% with J_{sc} of 8.65 mA.cm^{-2} while P3HT:PCBM:CC based device has exhibited the highest PCE of 3.59% with J_{sc} of 8.95 mA.cm^{-2}. The increase in the Jsc could be attributed to light-harvesting and effective charge transfer [43]. Generally, coumarin has sufficient fluorescence in the visible light range, good solubility and high quantum yield [44]. Extended conjugation in coumarin compound resulted in enhancement of solar cell efficiency. Electrons on trimethoxy groups in the coumarin were causing the conjugation to increase benzene ring and improving the electron transfer ability [45]. These special properties in the coumarin molecule also caused an increase in solar cell performance. The increase in the J_{sc} has been confirmed using internal power conversion efficiency (IPCE) measurements as shown in Fig. 8. All the devices have shown response spectra similar to the absorption spectra of their active layers with wide ranges from around 610 nm to 300 nm [46].

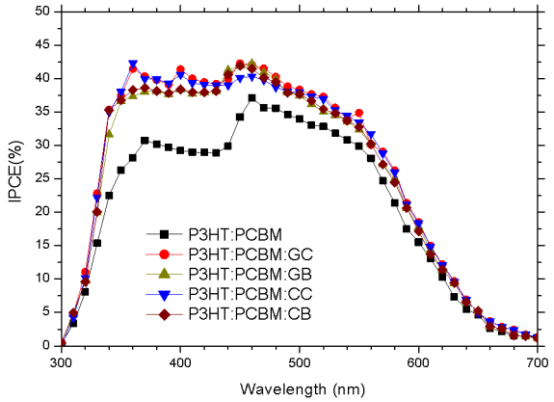

Figure 8. IPCE spectra of P3HT:PCBM-based solar cells and those of its ternary blends with GC, GB, CC and CB hybrids.

Table 1. Characteristics of P3HT:PCBM blended films with and without the addition of the GC, GB, CC and CB hybrids

	PURE	with GC	with GB	with CB	with CC
V_{oc} (V)	0.62	0.6	0.6	0.6	0.62
J_{sc} (mA.cm^{-2})	7.1	8.65	8.8	9.1	8.95
FF %	60	55	55	59	65
PCE %	2.62	2.85	2.9	3.22	3.59

Table 2. The photovoltaic parameters of the P3HT:PCBM:CC-based OSC.

Active later	P3HT:PCBM	P3HT:PCBM:CC
V_{oc} (V)	0.6	0.6
J_{sc} (mA.cm^{-2})	5.51	6.8
FF %	35	40
PCE %	1.16	1.62

As the best results have been achieved by using SWCNTs:Coumarin hybrids in P3HT:PCBM blend, the use of this ternary blend has been investigated for flexible OSCs using Indium tin oxide coated polyethylene terephthalate film (ITO-PET) as substrates, as shown in Fig. 9. The reference device based on P3HT:PCBM blend has shown a PCE of 1.16%, FF of 35%, J_{sc} of 5.51 mA.cm^{-2} and Voc of 0.6V. The J(V) characteristics of flexible solar cell of the reference and the hybrid-based devices, both in dark and under illumination, are demonstrated in Fig. 10. Using the SWCNTs:Coumarin hybrids within P3HT:PCBM blend has increase the device PCE to 1.62%, FF to 40% and J_{sc} to 6.8 mA.cm^{-2} as summarised in Table 2. These results clearly demonstrate that the new ternary hybrids are promising materials in improving the photovoltaic properties.

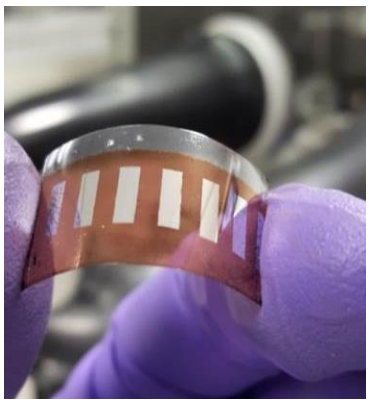

Figure 9. Photo of a flexible OSC based on P3HT:PCBM:CC active layer.

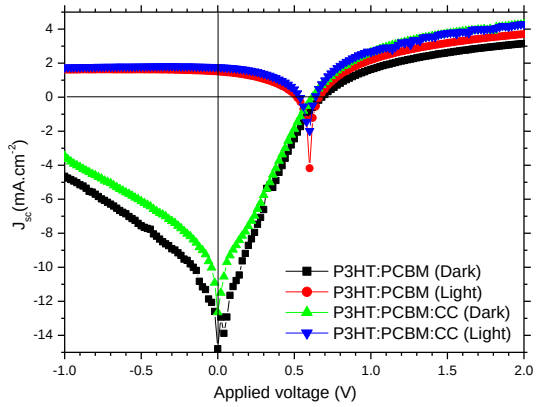

Figure 10. The J(V) characteristics of the pristine P3HT:PCBM and P3HT:PCBM:CC-based OSCs.

Conclusions

In the current study, thin films of P3HT:PCBM blended with the novel reduced graphene oxide:BODIPY (GB), reduced graphene oxide:Coumarin (GC), SWCNTs:BODIPY (CB) and SWCNTs:Coumarin (CC)) hybrid nanomaterials were prepared. The structures of the BODIPY and coumarin compounds were determined by FT-IR, 1H NMR, MALDI-TOF mass, cyclic voltammetry and UV–Vis, while their hybrid materials were characterized by FT-IR, Raman, UV–Vis spectroscopies and thermogravimetric analysis. The surface morphology of these hybrid films were determined by SEM. Absorption spectra of the hybrids in P3HT:PCBM blend showed higher variation in the absorption peak positions as compared to P3HT:PCBM. The Eg values were estimated using the Tauc equation in UV–Visible absorption spectra as 2.44 eV for BODIPY, 2.85 eV for coumarin, 2.39 eV for CB, 2.77 eV for CC, 2.37 eV for GB and 2.80 eV for GC. The highest value for the solar cell efficiency on ITO glass at 8.95 mA.cm^{-2} was calculated to be 3.59%. This corresponded to an increase of 37% efficiency with CC.

Conflicts of interest

There are no conflicts to declare.

Acknowledgements

Partial work (CC and CB) of this study was supported by a project from the Scientific and Technological Research Council of Turkey (TUBITAK) (Project number: 115Z734). We wish to thank TUBITAK ULAKBIM, High Performance and Grid Computing Center (TR-Grid e-Infrastructure) for the calculations reported in the theoretical part of this paper. T. Basova acknowledges the research fund by the Program of basic scientific research (Project number: V.44.4.3).

Notes and references

1 P. J. Reddy, Solar Power Generation: Technology, New Concepts & Policy. CRC Press, 2012.
2 N. L. Panwar, S. C. Kaushik and S. Kothari, *Renew. Sust. Energ. Rev.*, 2011, **15(3)**, 1513
3 T. Li, N. Ameri and C.J. Brabec, *Energ. Environ. Sci.*, 2013, **6(8),** 2390.
4 http://www.ecoworld.com/energy-fuels/how-much-solar-energy-hits-earth.html.
5 N. Manaf, Organic/inorganic Hybrid Solar Cells Based on Electroplated CdTe, Sheffield Hallam University. Materials Engineering Research Institute, degree granting institution. (2015).
6 S. Günes, H. Neugebauer and N.S. Sariciftci, *Chem. Rev.*, 2007, **107**, 1324.
7 D. Chalal, R. Garuz, D. Benachour, J. Boucle and B. Ratier, *Synth. Met*., 2016, **212**, 161.
8 J.A. Reinspach, Y. Diao, G. Giri, T. Sachse, K. England, Y. Zhou, C. Tassone, B.J. Worfolk, M. Presselt, M.F. Toney and S. Mannsfeld, *ACS Appl Mater. Inter.*, 2016, **8**, 1742.
9 Y.S. Kim, Y. Lee, J.K. Kim, E.O. Seo, E.W. Lee, W. Lee, S.H. Han and S.H. Lee, *Curr. Appl. Phys.*, 2010, **10**, 985.
10 M. F. De Volder, S. H. Tawfick, R. H. Baughman and A. J. Hart, *Science*, 2013, **339**, 535.
11 B. Kadem, A. Hassan, M. Göksel, T. Basova, A. Şenocak, E. Demirbaş and M. Durmuş, *RSC Advances*, 2016, **6**, 93453.
12 N. Boens, V. Leen and W. Dehaen, *Chem. Soc. Rev.*, 2012, **41**, 1130.
13 Y. Ni and J. Wu, *Org. Biomol. Chem.*, 2014, **12**, 3774.
14 L. Yao, S. Xiao and F. Dan, *J. Chem.*, 2013, **2013**, 697850.
15 L. Bonardi, H. Kanaan, F. Camerel, P. Jolinat, P. Retailleau and R. Ziessel, *Adv. Funct. Mater.*, 2008, **18**, 401.
16 A. Bessette and G. S. Hanan, *Chem. Soc. Rev.*, 2014, **43**, 3342.
17 R. L. Vekariya, J. V. Vaghasiya and A. Dhar, Organic *Electronics*, 2017, **48**, 291.
18 A. Coskun, E. Deniz and E.U. Akkaya, *Org. Lett.*, 2005, **7**, 5187.
19 S. Atilgan. T. Özdemir and E. U. Akkaya, *Org. Lett.*, 2010, **12**, 4792.
20 H. Yanık, M. Göksel, S. Yeşilot and M. Durmuş, *Tetrahedron Lett.*, 2016, **57**, 2922.
21 E.N. Kaya, F. Yuksel, G. Altınbaş Özpınar, M. Bulut and M. Durmuş, *Sensor Actuat. B: Chem.*, 2014, **194**, 377.
22 B. Kadem, M. Göksel, A. Şenocak, E. Demirbaş, D. Atilla, M. Durmuş, T. Basova, K. Shanmugasundaram and A. Hassan, Polyhedron, 2016, **110**, 37.
23 E.B. Orman, A. Koca, A.R. Özkaya, I. Gürol M. Durmuş and V. Ahsen, *J. Electrochem. Soc.*, 2014, **161**, H422.
24 M.J. Frisch, G.W. Trucks, H.B. Schlegel, G.E. Scuseria, M.A. Robb, J.R. Cheeseman, et al. Gaussian 09, Revision A.02 Gaussian, Inc., Wallingford CT, 2009.
25 A. D. Becke, *J. Chem. Phys.*, 1993, **98**, 5648.
26 G. Yue, J. Wu, Y. Xiao, H. Ye, J. Lin and M. Huang, *Chin. Sci. Bull.*, 2011, **56**, 325.
27 W. Ma, C. Yang, X. Gong, K. Lee and A.J. Heeger, *Adv. Funct. Mater.*, 2015, **15**, 1617.
28 B. Kadem, M.K. Al-Hashimi and A. Hassan, *Energy Procedia*, 2014, **50**, 237.
29 a) B. Ballesteros, G. de la Torre, C. Ehli, G.M.A. Rahman, F. Agullo-Rueda, D.M. Guldi and T. Torres, *J. Am. Chem. Soc.*, 2007 **129**, 5061. b) C. Casiraghi, A. Hartschuh, H. Qian, S. Pliscanec, C. Georgia, A. Fasoli, K.S. Novoselov, D.M. Basko, and A.C. Ferrari, *Nano Lett.*, 2009, **9**, 1433.
30 L. Alvarez, A. Righi, S. Rols, E. Anglaret, J.L. Sauvajol, E. Munoz, W.K. Maser, A.M. Benito, M.T. Martinez, G.F. de La Fuente, Physical Review B, 2001, 63, 153401; D. Huo, L. Yang, C. Hou, H. Fa, X. Luo, Y. Lu, X. Zheng, J. Yang and L. Yang, *Spectrochim. Acta A*, 2009, **74**, 336.

31 S. M. Polyakov, T.V. Basova, M. Göksel, A. Şenocak, E.Demirbaş, M. Durmuş, B. Kadem and A. Hassan, *Synth. Met.*, 2017, **227**, 78.
32 B. Ren, L. Zhu, G. Cui, Y. Sun, X. Zhang, F. Liang and Y. Liu, *Tetrahedron Lett.*, 2013, **54**, 5953.
33 G. Gritzner and J. Kuta, Pure & Appl. Chem., 1984, **56,** 461-466.
34 B. Kadem, A. Hassan, and W. Cranton, *J. Mater. Sci. Mater. Electron.*, 2016, **27**, 7038.
35 Y. Sun, J. Liu, Y. Ding, and Y. Han, *Colloid. Surface. A*, 2013, **421**, 135.
36 J. M. Holt, A. J. Ferguson, N. Kopidakis, B. A. Larsen, J. Bult, G. Rumbles and J. L. Blackburn, *Nano Lett.*, 2010, **10(11)**, 4627.
37 T. Salim, H. W. Lee, L. H. Wong, J. H. Oh, Z. Bao and Y. M. Lam, *Adv. Funct. Mater.*, 2016, **26(1)**, 51.
38 H. Klfout, A. Stewart, M. Elkhalifa and H. He, *ACS Appl. Mater. Inter.*, 2017, **9 (46)**, 39873.
39 S. Erten-Ela, Y. Ueno, T. Asaba and Y. Kubo, *New J. Chem.*, 2017, **41(18)**, 10367.
40 H. Klfout, A. Stewart, M. Elkhalifa, and H. He, ACS Appl. Mater. Interfaces 2017, **9**, 39873−39889.
41 P. Robaeys, F. Bonaccorso, E. Bourgeois, J. D'Haen, W. Dierckx, W. Dexters, D. Spoltore, J. Drijkoningen, J. Liesenborgs, A. Lombardo, A. C. Ferrari, F. V. Reeth, K. Haenen, J. V. Manca and M.Nesladek. *Appl. Phys. Lett.*, 2014, **105(8)**, 136.
42 H. Derbal-Habak, C. Bergeret, J. Cousseau and J. M. Nunzi, *Sol. Energ. Mat. Sol. C.*, 2011, **95**, S53.
43 X. Zhang, X. Pei, C. Liao, and L. Zou, *Res. Chem. Intermediat.*, 2017, **43(5)**, 2737.
44 R. L. Vekariya, J. V. Vaghasiya and A. Dhar, *Org. Electron.*, 2014, **48**, 291.
45 M.M. Jadhav, J.V. Vaghasiya, D.S. Patil, S.S. Soni and N. Sekar, New J. Chem., 2018, **42**, 5267-5275.
46 A. Hassan, B. Kadem and W. Cranton, Thin Solid Films, 2017, **636**, 760.